

Tracking the Missing Baryons in the Local Group

Fabrizio Nicastro*, Andreas Zezas*, Martin Elvis*, Smita Mathur†, Fabrizio Fiore‡,
Cesare Cecchi-Pestellini*, Douglas Burke*, Jeremy Drake*, Piergiorgio Casella*

**Harvard-Smithsonian Center for Astrophysics 60 Garden St, Cambridge MA 02138*

†*Astronomy Department, The Ohio State University, 43210, Columbus, OH, USA*

‡*Osservatorio Astronomico di Monteporzio, Via Osservatorio Via Frascati 33,
Monteporzio-Catone (RM), I-00040 Italy*

The number of detected baryons in the low-redshift Universe ($z \leq 1$) is far smaller than the corresponding number of baryons observed at higher redshift. According to hydrodynamical simulations for the formation of structure in the Universe^{1,2,3}, "missing baryons" can amount up to 2/3 of the total baryonic mass in the Local Universe and would have escaped identification so far, due to their high temperature and low density that make their detection challenging. Here we show that the dispersion of the 'high velocity' OVI absorbers (HV-OVI), from a UV survey of AGN, is minimized in the Local Group frame, and so the HV-OVI are strongly implicated as being due to primordial Warm-Hot Intergalactic Medium (WHIM) pervading our Local Group. We estimate that the total baryonic mass contained in this medium is of $\sim 10^{12} M_{\odot}$, similar to the combined mass of the two most massive virialized constituents of the Local Group (Andromeda and the Milky Way), and of the order of the mass required to dynamically stabilize the Local Group⁴.

The first evidence for an absorption system due to the WHIM has recently been discovered in the X-ray and UV spectra of the blazar PKS 2155-3045 obtained with the Chandra Low Energy Transmission Grating (LETG)⁶, and the Far-Ultraviolet Spectroscopic Explorer (FUSE)⁷. Clearly one line of sight is inadequate to fully define this absorbing medium. FUSE observations of 11 Active Galactic Nuclei (AGN) showed two types of $z \sim 0$ OVI absorbers, similar to those observed in PKS 2155-304: (1) Low Velocity OVI clouds (LV-OVI, $|v_{\text{LSR}}| < 100 \text{ km s}^{-1}$)^{8,9,10,11,12}; and (2) High Velocity OVI clouds (HV-OVI, $|v_{\text{LSR}}| > 100 \text{ km s}^{-1}$)^{13,14,15}. To further investigate the nature of these absorbers we have examined a larger sample of AGNs having publicly available data in the FUSE archive, allowing us to clearly identify HV-OVI component with diffuse gas in the Local Group. After a selection in signal-to-noise ratio (details in Fig. 1's caption), the final sample contains 54 different lines of sight with 45 detected OVI absorbers.

The OVI velocity distribution in the Local Standard of Rest (LSR) (Fig. 1, dashed histogram) shows a narrow peak between $\pm 100 \text{ km s}^{-1}$ (LV-OVI) with a much broader, roughly symmetric distribution (Fig. 1, solid histogram) extending to $\pm 550 \text{ km s}^{-1}$ (HV-OVI). The bimodality of this distribution suggests that LV- and HV-OVI systems belong to two different populations of absorbers, as previously pointed out by Savage et al.⁸, and Sembach et al.¹³ In the following we concentrate on the HV-OVI absorbers only, and defer a comparison and complete discussion of both LV and HV systems to a forthcoming paper (Nicastro et al., in preparation).

A plot in Galactic coordinates of the LSR velocity distributions for the HV (Fig. 2a, upper panel) absorption systems shows that the LSR velocities of the HV-OVI absorbers split the sky in two distinct halves (Fig. 2a): the hemisphere with $0^\circ \leq l \leq 180^\circ$ contains only HV-OVI lines with **negative** velocities, while the other hemisphere

contains mostly HV-OVI absorbers with **positive** LSR velocity. There are three exceptions, (at $l \sim 254^\circ$, $b \sim -65.8^\circ$, $l \sim 202^\circ$, $b \sim -21.1^\circ$, and $l \sim 225^\circ$, $b \sim -83.2^\circ$). of these, the first two lines of sight, however, contain the only two negative HV-OVI systems in our sample with LSR velocities very close to the threshold velocity of $|v_{\text{LSR}}| = 100 \text{ km s}^{-1}$, and so may well belong to the LV-OVI population. The remaining lies at very high latitude (where the concept of longitude becomes meaningless).

The systematic LSR velocity distribution of HV-OVI is strikingly similar to that shown by the Compact High Velocity Clouds of hydrogen (CHVCs,¹⁶), and is consistent with matter that is either: (1) counter-rotating, with respect with the Galaxy disk rotation, on orbits external to the sun's orbit, (2) at rest in the Galactic halo or (3) at rest in the intergalactic space surrounding the Galaxy. The range of radial LSR velocities of the HV-OVI ($100 < |v_{\text{LSR}}|^{\text{HV}} < 550 \text{ km s}^{-1}$) greatly exceeds the range of observed radial velocities in the Galactic disk or halo, suggesting that the Galaxy related options [(1) and (2)] are unlikely. Moreover some of the HV-OVI velocities exceed a plausible measure of the escape velocity from the Milky way¹⁷, as observed in CHVCs^{16,18,19}. Finally, clouds in the Galaxy's halo would probably be rotating on random orbits around the galaxy's center, as Globular Clusters do. The peculiar velocities of these clouds along these orbits would tend to randomize the apparent symmetry induced in the LSR by the circular motion of the Sun in the Galaxy for matter effectively at rest in the halo, as observed in Globular Cluster. An intergalactic origin is more consistent with the data.

The spatial distribution of the HV-OVI velocities in the LSR (Figure 2a), and the direction and amplitude of the average LSR velocity vectors (Table 1), demonstrate that the LSR is not a rest frame system for the HV-OVI clouds. This is confirmed by translations of the velocity distribution to other convenient rest frames: the Galactic Standard of Rest (GSR) and the Local Group Standard of Rest (LGSR). If the HV-OVI

absorbers were clouds of gas in the Galaxy's halo, one would expect the amplitude of the average velocity vector to be a minimum and close to zero in the GSR frame, and increase again for translation into the LGSR, where it should have amplitude and direction consistent with the motion of our Galaxy in the direction of the barycenter of the Local Group ($l = 147^\circ$, $b = -25^\circ$; ²⁰). This is not observed. On the contrary, the amplitude of the HV-OVI average velocity vector decreases monotonically from the LSR to the LGSR, at which point it is only $\langle |v_{\text{LGSR}}|_{\text{HV}} \rangle = 25 \text{ km s}^{-1}$ (Table 1), much smaller than the corresponding velocities in the LSR and GSR, and close to the FUSE resolution ($\sim 20 \text{ km s}^{-1}$ at 1032 Å). At the same time, the direction of the average vector becomes very poorly constrained (Table 1). Both the low value of the residual motion and the large dispersion in l and b of the average vector (Table 1) suggest that the LGSR is the rest frame of the HV-OVI absorbers. Moreover, the symmetry present in the LSR velocity distribution of the HV-OVI systems (Fig. 2a) disappears in the LGSR (Fig. 2b) and instead appears random, again suggesting that the LGSR is a privileged reference frame for the HV-OVI absorbers. This locates the population of HV absorbers in the intergalactic space of the Local Group.

There are several pieces of evidence, both observational and theoretical, supporting the identification of the HV systems with tenuous and diffuse Warm-Hot gas filling our Local Group. Recent ``constrained'' hydrodynamical simulations for the formation of structures in our own Supercluster Environment^{21,22} predict a major reservoir of baryons in the local environment in the form of WHIM filaments. The Local Group should be embedded in one of these filaments. The net motion of our Galaxy toward M 31, in the "local filament" (on average at rest in the LGSR), would produce an apparent bulk motion of the filament, towards our Galaxy, in the direction of M 31. This is similar to what is observed for the velocity field HV-OVI absorbers. The mean GSR velocity vector of the HV-OVI absorbers, has $l = 280^\circ$, $b = +38^\circ$, and $\langle |v_{\text{GSR}}|_{\text{HV}} \rangle = +60$

km s⁻¹ (Table 1). This corresponds to a vector with opposite sign (i.e. $\langle |v_{\text{GSR}}|^{HV} \rangle = -60$ km s⁻¹), and Galactic coordinates of $l = 80^\circ$, $b = -38^\circ$, quite close to the Galactic coordinates of M 31: $l = 121^\circ$, $b = -22^\circ$.

Estimates of the dynamical mass of our Local Group exceed by more than a factor of 2 the measured mass of its visible constituents (e.g. 4). A total mass of $\sim 10^{12}$ M_⊕ would be needed to stabilize, dynamically, the Local Group. From the combined analysis of the absorption features from highly ionized gas in the UV (HV-OVI) and X-ray (OVII, OVIII and NeIX) spectra of the blazar PKS 2155-304, Nicastro et al.⁵ concluded that this absorber has to fill the intergalactic space surrounding the Galaxy. This system has a density of the order of $n_e \sim 4-6 \times 10^{-6}$ cm⁻³, a column density of $N_H \sim 4.5 \times 10^{19} ([\text{O/H}]_{0.3})^{-1}$ cm⁻² (where $[\text{O/H}]_{0.3}$ is the O/H metallicity ratio in units of 0.3 times the solar value of 7.4×10^{-4} ,²³) and so a linear size along the line of sight of $D \sim 2-4 \times ([\text{O/H}]_{0.3})^{-1}$ Mpc. If this particular line of sight is representative of the entire Local Group WHIM, then assuming a transverse size of $1 \times ([\text{O/H}]_{0.3})^{-1}$ Mpc, gives a total baryonic mass of $0.6-2 \times ([\text{O/H}]_{0.3})^{-3} \times 10^{12}$ M_⊕, sufficient to stabilize the Local Group.

Additional evidence supporting the Local-Group origin for the HV-OVI comes from the velocity distribution of the neutral Hydrogen High Velocity clouds (HV-HI)²⁴ studied in the 21cm HI emission line, and in particular from the CHVCs¹⁶. The spatial distribution of CHVC velocities, in the LSR is strikingly similar to that of the HV-OVI absorbers, with two main concentrations in the direction of the barycenter, and the anti-barycenter of the Local Group¹⁶. In the Braun & Burton sample¹⁶, the dispersion of the radial velocities decreases for translations of the rest frame from the LSR to the LGSR, from $\sigma_{\text{LSR}}^{\text{CHVC}} = 175$ km s⁻¹ down to $\sigma_{\text{LGSR}}^{\text{CHVC}} = 88$ km s⁻¹. The same monotonic decrease is observed for the HV-OVI absorbers, for which $\sigma_{\text{LSR}}^{\text{HV-OVI}} = 45$ km s⁻¹ and $\sigma_{\text{LGSR}}^{\text{HV-OVI}} = 28$ km s⁻¹. Braun & Burton found that the reference frame that minimizes

the dispersion velocity of the CHVCs, has an apex vector with coordinates similar, but not coincident, to those of the LGSR apex vector. The slight difference suggests that CHVCs have a residual bulk motion in the LGSR. The vector resulting from the difference between the apex vectors of the LGSR and that of the reference frame in which the dispersion velocity of the CHVCs is minimum, has $l = 304$, $b = +58$. This is consistent, within the errors, with the direction of the residual average vector that we find for the HV-OVI absorbers in the LGSR (Table 1).

We then propose that the CHVCs are the cold, condensed component (possibly approaching our Galaxy's and/or M 31's halo) of a multiphase local IGM. The more diffuse and tenuous warm medium, pervading the whole Local Group, is responsible for the observed HV-OVI absorption, as well as the X-ray OVII, OVIII and NeIX absorption systems, provides the pressure needed to confine the cold phase existing under the form of CHVCs, and contains up to hundred times the total mass of the cold component¹⁶. The baryonic mass in the warm-hot phase can account for up to 100% of the "missing baryons" in our Local Group.

1. Cen, R., & Ostriker J.P., Where are the Baryons? *Astrophys. J.*, **514**, 1-6 (1999)
2. Hellsten U., Gnedin, N. Y., Miralda-Escude', J., The X-Ray Foresr: A New Prediction of Hierarchical Structure Formation Models. *Astrophys. J.*, **509**, 56-61 (1998)
3. Davé, R., et al., Baryons in the Warm-Hot Intergalactic Medium. *Astrophys. J.*, **552**, 473-483 (2001)
- 4 Kahn, F. D. & Woltjer, L., Intergalactic Matter and the Galaxy. *Astrophys. J.*, **130**, 705-717, (1959)
5. Nicastro, F., et al, Chandra Discovery of a Tree in the X-ray Forest towards PKS 2155-304: the Local Filament? *Astrophys. J.*, **573**, 157-167 (2002)
6. Canizares, C.R., Schattenburg, M.L., Smith, H.I., 1986, The high energy transmission grating spectrometer for AXAF., *SPIE*, **597**, 253,
7. Moos, H.W., et al., Overview of the Far Ultraviolet Spectroscopic Explorer Mission. *Astrophys. J.*, **538**, L1-6 (2000)
8. Savage B.D., et al., Far Ultraviolet Spectroscopic Explorer Observations of O VI Absorption in the Galactic Halo. *Astrophys. J.*, **538**, L27-30, (2000)
9. Wakker, B.P., et al., The FUSE Survey of Galactic OVI. *AAS*, **199**, 6508, (2001)
10. Savage et al., Distribution and Kinematics of OVI in the Milky Way Halo. *AAS*, **199**, 6504 (2001)

11. Howk, J.C., Savage, B.D., Sembach K.R., & Hoopes C.G., Far-Ultraviolet Spectroscopic Explorer observations of Degree-Scale Variations in Galactic Halo OVI *Astrophys. J.*, **572**, 264, (2002)
12. Hoopes, C. G., Sembach, K. R., Howk, J. C., Savage, B. D., Fullerton, A. W., A Far Ultraviolet Spectroscopic Explorer Survey of Interstellar O VI Absorption in the Small Magellanic Cloud. *Astrophys. J.*, **569**, 233-244 (2002)
13. Sembach, K.R. et al., Far Ultraviolet Spectroscopic Explorer Observations of O VI in High-Velocity Clouds. *Astrophys. J.*, **538**, L31-34 (2000)
14. Sembach, Pierce Prize Lecture: High Velocity Clouds: Cosmological and Galactic Weather. *AAS*, **199**, 11301, (2001)
15. Heckman, T.M., Norman, C.A., Strickland D.K., & Sembach K.R., On the Physical Origin of OVI Absorption-Line Systems. *Astrophys. J* in press ([astro-ph/020556](#)) (2002)
16. Braun, R. & Burton, W. B., The kinematic and spatial deployment of compact, isolated high-velocity clouds. *Astrophys. J.*, **341**, 437-450, (1999)
17. Oort, J. H., Asymmetry in the Distribution of Stellar Velocities. *The Observatory*, **49**, 302-304, (1926)
18. de Heij, V., Braun, R., Burton, W. B., High-Resolution Imaging of Compact High-Velocity Clouds (II). *Astron. Astrophys.*, in press, [astro-ph/0206333](#) (2002)
19. Blitz, L., Local Group HVCs: Status of the Evidence. In *Extragalactic Gas at Low Redshift*, ASP Conference Proceedings **Vol. 254**, 215 Eds. Mulchaey J.S. & Stocke J., San Francisco: Astronomical Society of the Pacific (2002)

20. Einasto, J., & Lynden-Bell, D., On the mass of the Local Group and the motion of its barycentre. *Mon. Non. R. Astron. Soc.*, **199**, 67-80 (1982)
21. Kravtsov, A.V., Klypin, A., & Hoffman, Y., Constrained Simulations of the Real Universe: II. Observational Signatures of Intergalactic Gas in the Local Supercluster Region. *Astrophys. J.*, in press, **astro-ph/0109077** (2002)
22. Klypin, A., Hoffman, Y., Kravtsov, A., Gottloeber, S., Constrained Simulations of the Real Universe: the Local Supercluster. *Astrophys. J.*, submitted, **astro-ph/0107104**, (2001)
23. Grevesse, N., & Anders, E., Solar-system abundances of the elements - A new table, in Cosmic abundances of matter, Proceedings of the AIP Conference, Minneapolis, MN, Sept. 7-9, *AIP Conference Proceedings*, **Vol. 183**, Ed. New York, American Institute of Physics, p. 1-8 (1989)
24. Blitz, L., Spergel, D.N., Teuben, P.J., Hartmann, D., & Burton, W.B., High-Velocity Clouds: Building Blocks of the Local Group. *Astrophys. J.*, **514**, 818-843 (1999)
25. Sankrit, R., Kruk, J. W., Ake, T. B., & Anderson B.-G., The FuseData Analysis Cookbook v. 1.0, (<http://fuse.pha.jhu.edu/analysis.cookbook.html>)
26. Freeman, P., Doe, S., Siemiginowska, A., Sherpa: a Mission-Independent Data Analysis Application. *SPIE*, **4477**, 76-87 (2001)

Acknowledgements

FN thanks G. C. Perola and P. Kaaret for fruitful discussions and useful comments. This work has been partly supported by NASA-Chandra grants GO2-3122A and the NASA-Chandra X-ray Center contract.

Correspondence and requests for materials should be addressed to F.N.

(fnicastro@cfa.harvard.edu)

Competing interests statement

The authors declare that they have no competing financial interests

Table 1

Average (v, l, b) vectors, and associated uncertainties, for the HV-OVI absorbers, in the LSR, GSR and LGSR. Averages and standard deviations are computed (a) projecting (v, l, b) onto three Cartesian axis (X,Y,Z), (b) averaging the Cartesian components and transforming back ($\langle X \rangle, \langle Y \rangle, \langle Z \rangle$) into ($\langle v \rangle, \langle l \rangle, \langle b \rangle$), (c) computing the standard deviation of the Cartesian components, and propagating the errors in quadrature to obtain uncertainties on ($\langle v \rangle, \langle l \rangle, \langle b \rangle$).

Reference Frame	$\langle v \rangle$ (km s ⁻¹)	$\langle l \rangle$ (deg.)	$\langle b \rangle$ (deg.)
LSR	125±15	276±10	30±21
GSR	60±10	280±18	38±41
LGSR	25±10	293±35	32±78

Figure 1

Histogram of the HV-OVI (solid line) and LV-OVI (dashed line) velocity distributions in the LSR. Among the 54 objects of our sample, 45 (83 %) show at least one clear OVI absorption component at $z \sim 0$ at our detection thresholds (7 out of the remaining 9 objects have poor quality FUSE spectra, with detection threshold of $\text{EW} \geq 200 \text{ m}\text{\AA}$). Of these 45 lines of sight, 38 show LV-OVI absorption (70% of the sample), and 32 (59% of the sample) show HV-OVI components, with 22 objects showing both. Only 3 lines of sight show multiple LV or HV absorption.

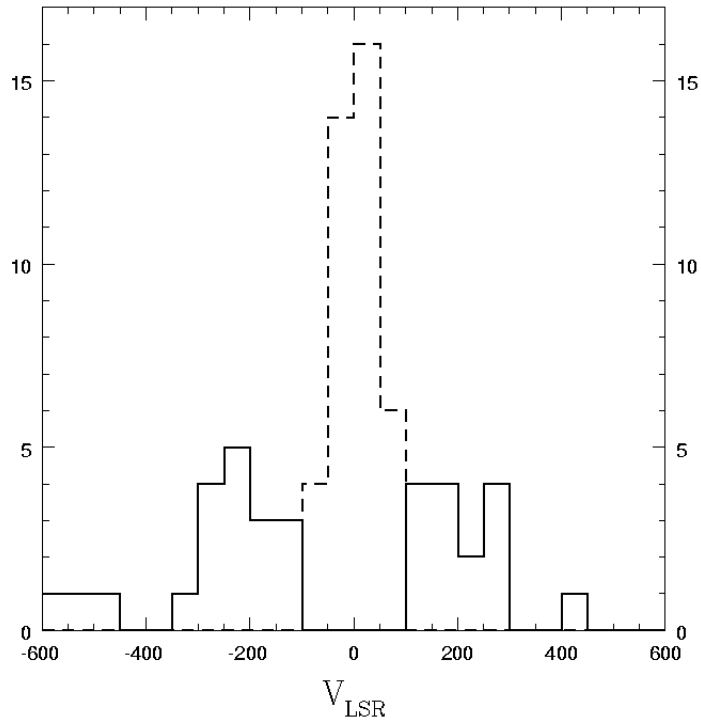
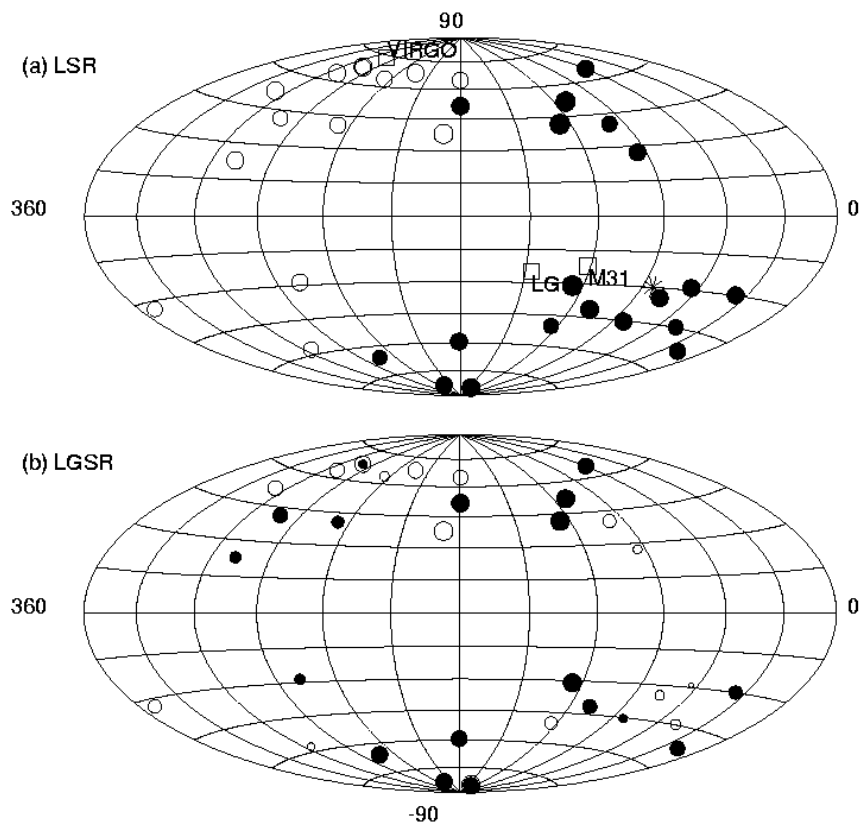


Figure 2

Aitoff plots of the (a) LSR and (b) LGSR velocity distributions for the HV-OVI absorption systems. In both panels filled circles correspond to negative velocities, while open circles correspond to positive velocities. In the upper panel the open squares indicate the position of (i) the barycenter of the Local Group (LG), (ii) M 31, and (iii) the Virgo cluster, as labeled. The star, instead, marks the position of the barycenter of the distribution.



Methodology

We used only data from the LiF mirror and the A1 detector segment, which have optimal efficiency in the waveband around the OVI line. The data were calibrated and cleaned following the procedures presented in the FUSE Data Analysis Cookbook²⁵. The resolution of the final data is $\sim 20 \text{ km s}^{-1}$, at 1032 Å.

We selected our sample based on a signal-to-noise ratio criterion. In particular, since we were interested in the OVI absorption lines at 1032 Å we concentrated only in spectra with signal-to-noise ratio (S/N) per resolution element of 35 in this spectral region. This selection reduced the initial sample to 54 different lines of sight, all with Galactic latitude $|b| > 20^\circ$ (because of the high extinction suffered by lines of sight crossing a significant portion of the Galactic disk). At this lowest quality spectra (S/N~35), absorption lines with equivalent width (EW) larger than $\sim 200 \text{ m}\text{\AA}$ are detected at $> 3 \sigma$, while the highest signal-to-noise spectra in our sample guarantee the detection of absorption lines down to EW $\sim 20 \text{ m}\text{\AA}$.

For each $z \sim 0$ OVI absorption line spectrum we used the CIAO fitting engine "Sherpa"²⁶ to fit a power law continuum and negative Gaussians to represent the absorption lines and derive the best fit wavelength and width. In all cases, we fitted only a narrow portion of the continuum from 1028.5 Å to 1034 Å.

We also looked for possible contamination by H₂ absorption lines from the interstellar medium of our Galaxy using H₂ templates that we computed for excitation (non-LTE cases) temperatures between 80 and 120 K, densities of 10, 50 and 100 cm⁻³, and Doppler parameters of 3, 10 and 20 km s⁻¹. In the wavelength range of interest we looked for the presence of the two strong H₂ (6-0) P(3) $\lambda 1031.19 \text{ \AA}$ and R(4) $\lambda 1032.35 \text{ \AA}$

Å lines. We verified that spectra along lines of sight with equivalent hydrogen column densities lower than $\sim 2 \times 10^{20} \text{ cm}^{-2}$ show only weak H₂ absorption. Spectra along lines of sight with $N_{\text{H}} > 2 \times 10^{20} \text{ cm}^{-2}$, instead, show usually strong P(3) $\lambda 1031.19 \text{ \AA}$ and R(4) 1032.35 \AA absorption. The P(3) $\lambda 1031.19 \text{ \AA}$ and R(4) 1032.35 \AA lines occur at velocities of -214 and +123 km s⁻¹, and so may potentially contaminate HV-OVI lines. We found that about 30% of the negative HV-OVI lines and less than 20% of the positive HV-OVI lines had profiles contaminated by the P(3) $\lambda 1031.19 \text{ \AA}$ and R(4) 1032.35 \AA lines respectively. In these cases we used other strong H₂ lines in relatively featureless portions of the FUSE spectra, to clearly determine the bulk velocity of the H₂ absorber, and so disentangle the HV-OVI line from the contaminating H₂. In particular we used the (6-0) P(2) $\lambda 1028.10 \text{ \AA}$ and R(3) $\lambda 1028.98 \text{ \AA}$ lines, shortward of the OVI $\lambda 1031.926 \text{ \AA}$ line, and the (1-0) P(2) $\lambda 1040.36 \text{ \AA}$ and (5-0) R(3) $\lambda 1041.16 \text{ \AA}$ lines, longward. Only in 2 cases could the presence of the HV-OVI line not be safely established, and so we considered those two lines of sight as free from HV-OVI absorption, at our detection threshold. In three more cases the presence of the HV-OVI line was clearly established, but its position and width only poorly constrained.